

Cryogenic buffer-gas loading and magnetic trapping of CrH and MnH molecules

Michael Stoll,¹ Joost M. Bakker,^{2,3} Timothy C. Steimle,⁴ Gerard Meijer,¹ and Achim Peters²¹*Fritz-Haber-Institut der Max-Planck-Gesellschaft, Faradayweg 4-6, 14195 Berlin, Germany*²*Institut für Physik, Humboldt Universität zu Berlin, Hausvogteiplatz 5-7, 10117 Berlin, Germany*³*FOM Institute for Plasma Physics Rijnhuizen, Postbus 1207, 3430 BE Nieuwegein, The Netherlands*⁴*Department of Chemistry and Biochemistry, Arizona State University, Tempe, Arizona 85287, USA*

(Received 20 June 2008; published 17 September 2008)

We report on the buffer-gas cooling and trapping of CrH and MnH molecules in a magnetic quadrupole trap with densities on the order of 10^6 cm^{-3} at a temperature of 650 mK. Storage times of up to 180 ms have been observed, corresponding to a 20-fold lifetime enhancement with respect to the field-free diffusion through the ^3He buffer-gas. Using Monte Carlo trajectory simulations, inelastic molecule- ^3He collision cross sections of 1.6×10^{-18} and $3.1 \times 10^{-17} \text{ cm}^2$ are extracted for CrH and MnH, respectively. Furthermore, elastic molecule- ^3He collision cross sections of $1.4(\pm 0.5) \times 10^{-14} \text{ cm}^2$ are determined for both species. We conclude that the confinement time of these molecules in a magnetic trapping field is limited by inelastic collisions with the helium atoms leading to Zeeman relaxation.

DOI: [10.1103/PhysRevA.78.032707](https://doi.org/10.1103/PhysRevA.78.032707)

PACS number(s): 34.50.-s, 34.80.Bm, 37.10.Pq

I. INTRODUCTION

Research in the field of cold molecules has experienced an enormous growth over the past few years due to the possibility to test concepts of fundamental physics and the promise for studying new effects. Among the precision experiments are the possibility to measure an upper limit to a predicted dipole moment of the electron (edm) [1,2] or the time variability of fundamental constants [3,4]. Control over the collision energy in low-temperature collisions also opens up a new way of studying individual structures and interactions between the collision partners [5] and might lead to observation of new chemical reaction pathways [6,7]. In addition, trapped molecules have been proposed as an ideal system for realizing qubits, a key step toward quantum computing [8,9].

To obtain dense samples of cold molecules, numerous methods have been developed. Some of them are based on the formation of molecules from trapped ultracold atoms, either through photoassociation [10] or by tuning through magnetic Feshbach resonances [11]. Direct cooling and trapping of molecules can be achieved via Stark deceleration and subsequent electric trapping of polar molecules in a molecular beam [12], Stark-filtering of an effusive beam [13], collisions in crossed molecular beams [14], or buffer-gas cooling of molecules [15]. Among these approaches, buffer-gas cooling, which relies on the thermalization of the species of interest with a cold inert buffer gas, is the most general cooling method, as it is applicable to virtually all atomic and molecular species. It also offers the benefit of producing very large samples at sub-Kelvin temperatures, which can form a good starting point for further cooling by other techniques, such as evaporative cooling. The combination of this technique with magnetic trapping was pioneered by Doyle and co-workers and has been successfully applied to trap a large variety of paramagnetic atoms [16–19]. It also formed the basis of the first experiment where large samples of cold neutral molecules were confined in an external trapping field [15]. The technique was successfully extended to NH and ND, of which both have been trapped for several 100 ms at densities of $\sim 10^8 \text{ cm}^{-3}$ [20].

Collisions between the buffer-gas atoms and the molecular system under study, however, severely limit the number of molecular species that can be magnetically trapped after buffer-gas cooling. Compared to atoms, the probability for molecules to be scattered into untrappable states through collisions with the buffer-gas atoms is generally much higher. Such collisions lead to trap losses at rates that can preclude the complete isolation of the trapped molecular sample. This isolation is, however, needed for further cooling by controlled evaporation. The few experimental and theoretical studies of inelastic collisions in buffer-gas cooling and magnetic trapping so far indicate that the spin-spin and spin-rotation interactions play a decisive role in shifting the balance between unfavorable inelastic collisions and elastic collisions upon which the technique relies for thermalization [21–23]. Unfortunately, such studies have so far been limited to molecules with a $^2\Sigma$ or $^3\Sigma$ ground state. To investigate the scope of molecular systems that are amenable for buffer-gas cooling and magnetic trapping, we set out to obtain information about molecules with different ground states. In a previous publication [24], we described criteria to identify candidate systems for such a study. Based on these criteria, we selected two molecules with high-spin ground states, CrH and MnH, possessing a $^6\Sigma^+$ and a $^7\Sigma^+$ ground state, respectively. Due to their high multiplicity, they possess large magnetic moments ($5\mu_B$ for CrH and $6\mu_B$ for MnH) that make them suitable for magnetic trapping at our magnetic field strengths, which are on the order of 2 T. At the same time, their relatively small spin-spin and spin-rotation coupling constants, combined with a large rotational constant, indicate that they might possess a favorably high ratio between elastic- and inelastic-scattering cross sections for collisions with helium. Both molecules have strong electronic transitions in the visible wavelength range, allowing for efficient spectroscopic detection. Moreover, we found that both hydrides are straightforward to produce via laser ablation from solid precursor targets, a method particularly well suited for implementation in a cryogenic environment [24].

Here we report on our buffer-gas loading experiment, aiming at the investigation of the potential to extend this technique to molecular species with ground states of a high

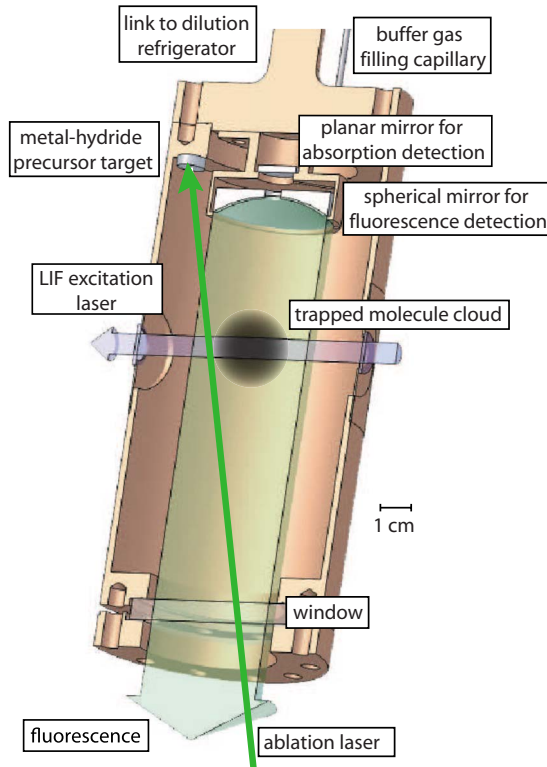


FIG. 1. (Color online) Scheme of the experimental setup, depicting a cut through the copper experimental cell. A hole in the spherical mirror to a planar mirror above allows for detection via absorption.

multiplicity. We have successfully trapped chromium monohydride and manganese monohydride molecules. Severe limitations on the storing times, however, are given by inelastic collision-induced Zeeman relaxation with the buffer-gas atoms. These processes are investigated using a simulation of the cooling and trapping dynamics of the molecule ensemble. By fitting this simulation to our measurements, inelastic collision cross sections for both molecules are determined, and the details and limitations of cooling and trapping both molecules using this technique are studied. In addition, the elastic molecule- ^3He collision cross sections are determined using measurements of the field-free diffusion times.

II. METHOD AND EXPERIMENTAL SETUP

The experiments are performed in a slightly modified version of the experimental setup described earlier [24]. A cylindrical experimental cell, made from oxygen-free high conductivity copper (OFHC), is attached and thermally anchored to the mixing chamber of a dilution refrigerator. The thermal link between refrigerator and experimental cell is formed by a 10-cm-long, 15-mm-diam copper rod forming a well-defined thermal impedance (see Fig. 1). In this configuration, the cell can be cooled to a base temperature of 100 mK. The cell is surrounded by a superconducting magnet in anti-Helmholtz configuration that consists of two coils of NbTi/Cu wire spun onto a titanium bobbin designed to with-

stand the repulsive forces of the two coils. This magnet produces a maximum trapping field of ~ 2 T at the cell boundaries, with a local field minimum in the center of the buffer-gas cell. Optical access to the trapping center is provided by a 50-mm-diam window sealing the bottom of the cell and, different from our previous experiments, by two 12.5-mm-diam sapphire windows with an effective aperture diameter of 9 mm in the side wall of the cell body. As the effective trap edge in the radial direction coincides with the cell wall, the design of the optical access on the side is aiming to minimize the cell wall thickness. For this reason, the side windows are glued using epoxy (Stycast 2850) onto a 0.1-mm-thick copper foil, which itself is glued to the cell wall covering 25-mm-diam openings. The thin copper foil serves to relieve the mechanical stress on the glue joints and the sapphire window resulting from thermal contraction when the apparatus is cooled down from room temperature. RuO thermistors and a resistive heater within the cell body are used to monitor and control the temperature of the cell.

Molecules are injected into the cell via laser ablation from a solid precursor. For this, light pulses produced by a Q -switched pulsed Nd:YAG laser (Continuum Minilite-II, 532 nm, ~ 12 mJ) are steered and loosely focused with a 750 mm focal distance lens onto the precursor targets glued to the top of the buffer-gas cell. These targets are solid Cr (Mn) chips that are electrochemically doped with H atoms. To prepare these targets, the chips (size: ~ 1 cm 2) are submerged in distilled water and a negative potential (~ 20 V) with respect to a platinum counter electrode is applied. To increase the conductivity of the solution, H_2SO_4 is added until a current of ~ 100 mA between the two electrodes is reached; this current is then maintained for 1 h. This procedure results in the embedding of hydrogen in the interstitial sites of the Cr (Mn) crystal [25]. Since Mn suffers from dissolution by the acid, care is taken to minimize this effect while reaching the necessary current by carefully adjusting the H_2SO_4 concentration. When gluing the targets into the buffer-gas cell, it is difficult not to expose them to air for a few hours. However, we found that this does not affect the yield for both molecules in the ablation process.

After ablation, the molecules are cooled by the helium buffer-gas atoms. In the current experiment, we use ^3He because it has a higher vapor pressure than ^4He at our operating temperatures of $T < 1$ K. This allows for buffer-gas loading at lower temperatures with a higher effective trap depth $\eta = \mu B / k_B T$, where μ is the effective magnetic moment of the molecules, B is the magnetic field strength, k_B is the Boltzmann constant, and T is the Boltzmann temperature of the molecule sample. Moreover, excess ^3He gas is more easily extractable from the experimental cell by pumping on the filling capillary. The disadvantage of the use of ^3He with the present cooling power of the dilution refrigerator is that a thermal disconnect from the cell wall is more difficult to obtain; however, it will be shown below that this is irrelevant as the trapping times observed are too short to establish a thermal disconnect by freezing the helium to the cell walls.

Optical detection of the molecules in the trapping region is performed using laser-induced fluorescence (LIF). To this end, a pulsed excitation laser is sent through the cell using the two side windows. Fluorescence produced by the mol-

ecules is collected by a 35-mm-diam spherical silver mirror attached to the top of the experimental cell. The radius of curvature of the silver mirror is chosen such that the 35 mm distance focal point of the mirror coincides with the center of the trapping field. Outside the cryostat, the reflected fluorescence is imaged onto a photomultiplier tube (PMT, Hamamatsu R943-02) by means of a planar silver mirror, a lens, and an interference filter appropriate for the wavelength of the detected light (spectral width: 20 nm). To shield the PMT against the stray fields produced by the superconducting magnet, the cathode array is surrounded by a single-layer μ -metal shield. The PMT output current is converted into a voltage using a 50 Ω resistor and integrated using a 12-bit 100 MS/s digitizer (Acqiris DC438). For the magnetic trapping experiment of CrH, the PMT current is directly amplified using a fast preamplifier (Ortec VT120A) to perform photon counting, using the same digitizer. The latter allows for obtaining more precise information on the quantity of molecules within the detection area. Unfortunately we cannot do this for MnH, since the lifetime of the excited state of this molecule is ~ 10 times smaller (~ 100 ns) and, as a consequence, single photons in some cases would not be resolved with our digitizer. To obtain information on the time dependence of the number of molecules in the trapping region, the time delay between the ablation and excitation pulses is varied using a home-made delay generator.

CrH molecules are detected using LIF via excitation of the $R_1(0)$ rotational transition of the $A^6\Sigma^+(v'=1) \leftarrow X^6\Sigma^+(v''=0)$ band system near 766 nm. Fluorescence into the $X^6\Sigma^+(v''=1)$ state near 860 nm is collected [26]. The 766 nm light is produced by a pulsed dye laser system (Spectra-Physics PDL-3, LDS 751 dye) pumped by a frequency-doubled Nd:YAG laser (Spectra-Physics INDI). With this system, 766 nm light pulses of ~ 5 mJ and a bandwidth of ~ 0.1 cm^{-1} are produced. The dye laser is not actively wavelength stabilized, but since the spectral width of the excitation laser is rather large, small drifts of the wavelength do not substantially affect our measurements.

MnH molecules are detected via excitation of the $A^7\Pi(v'=0, N'=0, J'=2) \leftarrow X^7\Sigma^+(v''=0, N''=0, J''=3)$ rotational transition near 568 nm and collection of fluorescence into the $X^7\Sigma^+(v''=1)$ state near 624 nm [27]. The excitation light is created by a second pulsed dye laser system, identical to the one for CrH, now with Rhodamine 6G dye.

To allow for a measurement of the buffer-gas density, the experiment is also equipped to perform absorption spectroscopy on a sample of buffer-gas cooled chromium atoms, which are also produced by laser ablation in the cell. To this end, a planar silver mirror is placed directly above the spherical mirror for fluorescence collection. Both the spherical mirror inside the experimental cell and the planar mirror outside for imaging the fluorescence onto the PMT have a 5 mm hole to allow for the entrance and exit of an absorption detection laser. The procedure for atomic chromium detection is identical to that used in our previous publication [24]. The helium density is then determined indirectly via a measurement of the field-free lifetimes of chromium atoms within the copper cell. This diffusion time can be translated into a buffer-gas density with the help of an analytic model that describes the diffusion of two gases through each other

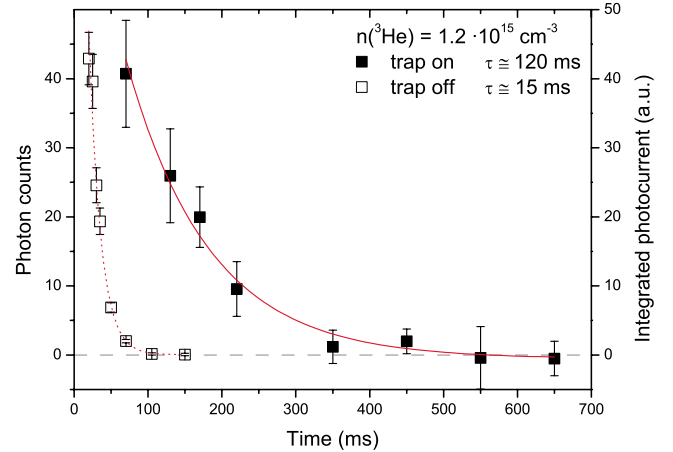


FIG. 2. (Color online) Time dependence of the fluorescence signal from CrH molecules after injection into the buffer-gas cell in the presence (solid squares: photon counts) and absence (open squares: integrated photocurrent) of the magnetic trapping field at a buffer-gas density of $1.2 \times 10^{15} \text{ cm}^{-3}$. Each data point represents the average of five measurements.

if the elastic collision cross section for Cr- ^3He is known [28,29]. At a temperature of 300 mK, this cross section was measured to be $1.8(\pm 0.6) \times 10^{-14} \text{ cm}^2$ [30]. From the spectral line shapes of the field-free chromium measurements, we determine our buffer-gas temperature to be ~ 650 mK. Assuming that the elastic collision cross section is the same at this slightly higher temperature, we convert the measured Cr diffusion time to a buffer-gas density with the model mentioned above. The error on the helium density is then governed by the error in the elastic collision cross section and is estimated to be about 30%.

III. RESULTS AND DISCUSSION

To investigate the collisional properties of CrH and MnH molecules, and the possibility to magnetically trap these molecules under buffer-gas loading conditions, it is necessary to obtain both the inelastic- and the elastic-scattering cross sections for collisions between helium atoms and the molecules. To this end, the diffusion lifetimes of a sample of molecules for a series of buffer-gas densities, with and without the magnetic trapping field, are measured. Apart from a direct observation of trapping, these measurements allow for extraction of the molecular elastic collision cross sections with ^3He if the buffer-gas density is known.

In Fig. 2, an example of such a measurement is depicted for CrH at a buffer-gas density of $n=1.2 \times 10^{15} \text{ cm}^{-3}$. It shows a measurement of the detected fluorescence signal, produced at various delays between the ablation and detection laser pulses, both with the magnetic trapping field on and off. Each value in this curve is the mean value of five subsequent measurements of the fluorescence signal for a specific time delay between ablation and excitation. To account for the degrading precursor targets, a (pseudo)random sequence of time delays is used. A single exponential decay function is then fitted to the averaged values, yielding a dif-

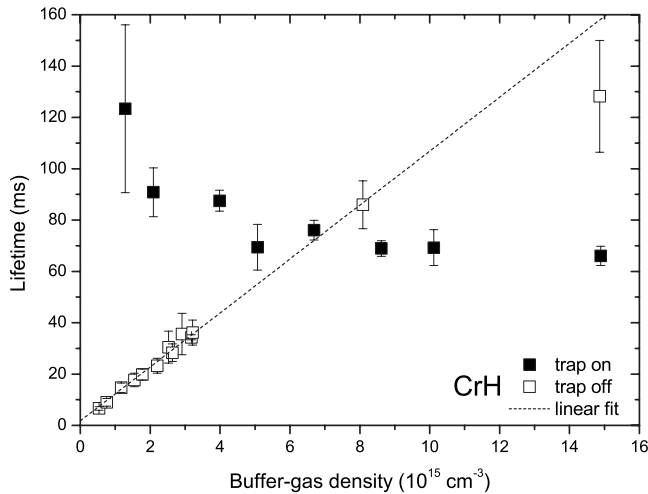


FIG. 3. Buffer-gas density dependence of the CrH lifetime in the presence (solid squares) and absence (open squares) of the magnetic trapping field. The dashed line is a linear fit of the field-free diffusion times excluding the point at the largest buffer-gas density.

fusion time constant. In the case, where the diffusion time is significantly enhanced by the presence of the magnetic field, we denote this as a trapping time.

From Fig. 2, it is immediately apparent that the magnetic field enhances the diffusion time of the molecules by a factor of ~ 10 , giving a clear signature of trapping. Given our photon collection efficiency of $\sim 0.1\%$, we estimate on the order of 10^5 molecules in the center of our trapping field at a density of $\sim 10^6 \text{ cm}^{-3}$ at 100 ms after injection via the ablation pulse.

To investigate collisional properties for CrH, the diffusion time is measured for a number of buffer-gas densities, both with and without the trapping field present. The results of these measurements are depicted in Fig. 3. The error bars on the lifetimes are dominated by shot-to-shot fluctuations in the fluorescence signal. This signal instability is on the order of 50% and arises from the molecule production method via laser ablation. The possibility to reduce the statistical errors by recording many data points is, however, restricted by the cooling power of the refrigerator since it takes on the order of 40 s to cool the cell from the heat of each ablation pulse. In the absence of the magnetic field, one clearly recognizes a linear dependence of the diffusion time on the buffer-gas density, which is fully consistent with a simple model of the diffusion process. From this linear dependence of the diffusion time constant, an elastic collision cross section for $^3\text{He-CrH}$ collisions of $1.4(\pm 0.5) \times 10^{-14} \text{ cm}^2$ is extracted. It is important to note that the error is dominated by the uncertainty in the buffer-gas density, which itself is limited by the uncertainty in the elastic cross sections for the $^3\text{He-Cr}$ collisions, as mentioned above.

In the presence of the magnetic trapping field, the dependence of the lifetime on the buffer-gas density is much more complicated. While the field-free diffusion time rises linearly with increasing helium density, in the trapping field the longest storage times are found for the lowest buffer-gas densities. Adding more helium, the trapping time decreases and for densities higher than $7 \times 10^{15} \text{ cm}^{-3}$ becomes shorter than

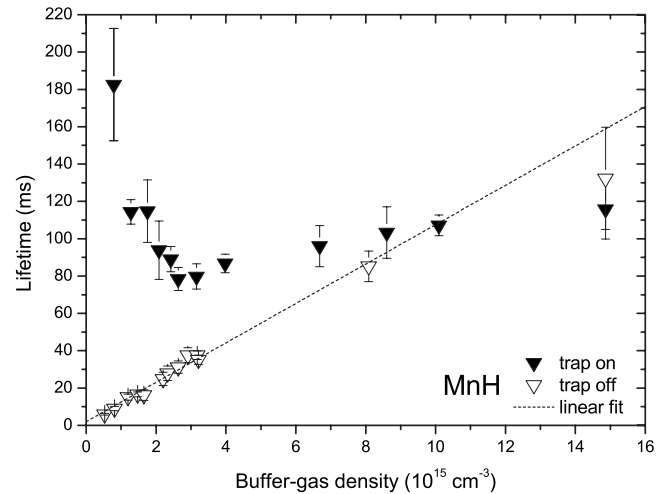


FIG. 4. Buffer-gas density dependence of the MnH lifetime in the presence (solid triangles) and absence (open triangles) of the magnetic trapping field. The dashed line is a linear fit of the field-free diffusion times excluding the point at the largest buffer-gas density.

the field-free diffusion time. This behavior is a strong indication for trap loss due to Zeeman relaxation. Although the addition of more buffer gas leads to cooling of a larger number of molecules, simultaneously the number of inelastic collisions that change the spin states of the particles is increased. If these spin flips transform a significant fraction of molecules into high-field seeking states, their lifetime in the presence of a trapping field is reduced. Since, on the other hand, such collisions do not affect the field-free diffusion, the lifetime in the trapping field can become smaller than in the field-free case.

The maximum trapping time of 120 ms is observed at a buffer-gas density of $1.2 \times 10^{15} \text{ cm}^{-3}$. At lower buffer-gas densities, the fluorescence signal is too weak to record a clear diffusion signal. It is likely that at densities below $1.2 \times 10^{15} \text{ cm}^{-3}$, the number of helium-CrH collisions is insufficient to translationally and rotationally cool a substantial fraction of the injected hot CrH molecules.

In Fig. 4, the same measurements as described above are depicted for MnH. The error bars for the data in the presence of the magnetic trapping field are somewhat larger for MnH than for CrH, which is partly due to the use of photon counting for CrH. From the field-free diffusion time for MnH, we find the same value for the elastic collision cross section of $1.4(\pm 0.5) \times 10^{-14} \text{ cm}^2$ as for CrH. The dependence of the “trapping” time on the buffer-gas density is also similar to that for CrH. Interestingly, however, where the trapping time for CrH monotonously falls with increasing buffer-gas density, for MnH it goes through a minimum at a density of $\sim 2.5 \times 10^{15} \text{ cm}^{-3}$ after which the lifetime increases again.

This rather counterintuitive effect can be explained as follows: an increased density of the buffer gas will lead to an increase in the number of collisions that leave a particle in a high-field seeking state and should result in a larger trap loss and a decreased lifetime. However, inelastic collisions can also transfer particles from a high-field seeking into a low-field seeking (trappable) state. If the buffer-gas density gets

to the point where the average time between collisions becomes smaller than the time it takes the particle to escape to the cell wall, a competition between spin-flip collisions leading to trap loss and spin-flip collisions from untrappable to trappable states starts to set in. If many molecules of the ensemble are transferred to low-field-seeking (trappable) states and back, this leads to an elongation of the lifetime because on average the atoms behave as in a state that is not sensitive to the magnetic field at all. This observed enhancement thus indicates a substantially larger inelastic collision cross section for MnH than for CrH.

The dependence of the trapping time of CrH on the buffer-gas density is very similar to that measured for NH by Doyle and co-workers [20]. For NH, a similar maximum trapping time of 200 ms was found, although this was measured at a lower trap depth than used in the experiment described here. At our buffer-gas temperature of ~ 650 mK, we have an effective trap depth $\eta \sim 10$. In the NH experiment, effective trap depths below $\eta = 7$ were used [20]. Since the trapping time in the absence of inelastic collisions exponentially grows with η , this points to a less favorable ratio of elastic to inelastic helium collision cross sections for CrH than for NH.

To quantify the latter statement, we performed trajectory simulations for CrH, MnH, and NH molecules in a buffer-gas experiment. For this, we use a Monte Carlo approach where the injection process is simulated by an initially uniform distribution of molecules over the trapping region. The molecules are given starting velocities described by a Maxwell-Boltzmann distribution at an initial temperature of 1000 K, and are uniformly distributed over all existing m_J levels. Rotational cooling is not simulated as all molecules are assumed to populate the rotational ground state. This is a simplification, since at typical initial temperatures of ~ 1000 K, hardly any molecules do populate these states. However, in buffer-gas cooling experiments at 4 K we find that more than $\sim 95\%$ of the molecules are cooled to the rotational ground state within 10 ms, and we typically only perform our measurements with time delays > 10 ms between ablation laser and detection laser. A further simplification is the assumption that the ^3He gas represents a thermal bath that never heats up.

The trajectory of each molecule is solved by integrating Newton's equations of motion until the next collision event, a specified end time, or until the molecule escapes from the cell volume. The mean time between collision events τ depends on the buffer gas density n , the mean relative velocity between the collision partners v_{rel} , and the elastic collision cross section σ_{el} , according to $\tau = 1/(n\sigma_{\text{el}}v_{\text{rel}})$. The collisions take place between the molecule and a ^3He atom with random velocity components consistent with a Maxwell-Boltzmann distribution at the specified temperature. Depending on the ratio of the elastic and inelastic collision cross section, there is a certain probability for a collision to be treated as either elastic or inelastic. No calculations for the inelastic collision cross section for CrH and MnH with helium exist. However, for NH and CaH a sharp rise in the inelastic collision cross section as a function of collision energy over several orders of magnitude is predicted [21,22]. In the case of NH, this rise is right at collision energies typical

for our experiment ($E > 0.1 \text{ cm}^{-1}$). It is not unlikely that such a rise, which is related to shape resonances in molecule- ^3He collisions, is also present for MnH and CrH. To account for this in a simple model, we implement the inelastic collision cross section as a step function: if the collision energy is below a certain energy barrier E_b , the inelastic collision cross section is zero, otherwise it is a nonzero constant. We further simplify by neglecting any magnetic field dependence of the elastic and inelastic collision cross sections. A third choice concerns the selection on accessible m_J states. We perform simulations both with inelastic collisions restricted to neighboring Zeeman levels ($m_J = \pm 1$) and with inelastic collisions to all Zeeman levels ($\Delta m_J = \text{all}$). In each case, the collision energy must be sufficient to overcome the energy difference between the initial and final Zeeman states.

For a given inelastic collision cross section σ_{inel} , the time dependence of the density of molecules in the center of the trapping region is extracted from the simulation. This calculated lifetime is then compared to the measured molecule lifetimes. A best value for σ_{inel} is then obtained by minimizing χ^2 . This is done for several values of the inelastic collision energy barrier E_b and for each choice of transitions allowed in inelastic collisions.

The model was successfully tested by simulating the trapping time dependence of NH molecules in the recent experiments by Doyle and co-workers [20]. The current simulations yield a good agreement in the functional shape of the buffer-gas density dependence of the trapping time and reproduce the measured values for the inelastic cross sections.

Figures 5 and 6 show the results of the simulation for CrH and for MnH, respectively. In each of the figures, the best fit to the trapping time dependence on buffer-gas density is given for a few collision energy barriers E_b . The results are shown for the model where inelastic collisions are restricted to neighboring Zeeman states ($\Delta m_J = \pm 1$, top graphs), as well as for the model where all energetically accessible Zeeman states are reachable in a single spin-flip process. For both molecules, the resulting inelastic collision cross sections are substantially larger for the "neighboring-states" model than for the "all-inclusive" model. This is readily explained by the fact that in the "all-inclusive" model ($\Delta m_J = \text{all}$), a change from a trapping into a nontrapping state can be induced by one single collision, while in the "neighboring state" model it requires at least four collisions for an $m_J = 3$ state to become nontrappable.

A second common feature is the rise in trapping time at large helium densities for a higher collision energy barrier E_b . This can be explained as follows: while inelastic collisions can bring a molecule into an untrappable, high-field seeking state, the reverse can also happen. This last process can only take place if the collision energy is sufficient to transfer the molecule to the higher-energy state. Raising E_b , and thus requiring a higher collision energy to produce a spin flip in the first place, eliminates all inelastic collisions at energies below E_b . This includes those that typically induce transitions to lower energy and therefore less trappable states. As a consequence, the relative probability for a collision to transfer the molecule into a higher-energy (more trappable) Zeeman state is increased. Since the average time between two spin-flip collisions at high buffer-gas densities can

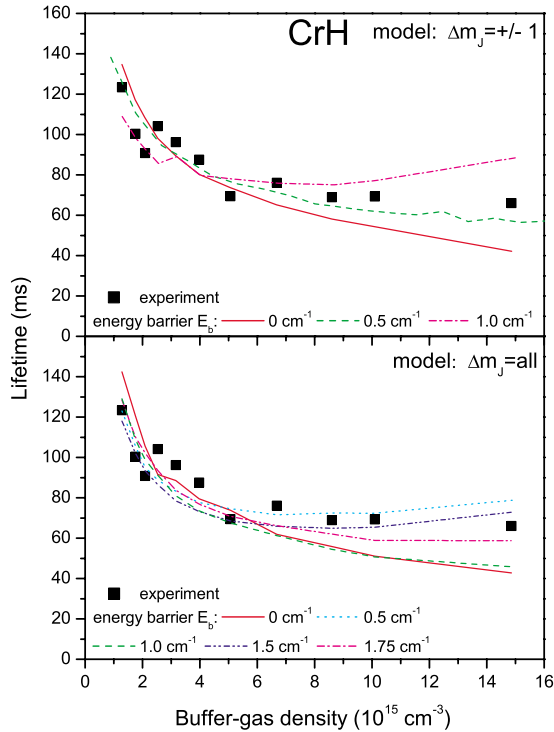


FIG. 5. (Color online) Simulated lifetime dependencies on the buffer-gas density of CrH, for two variants of the spin-flipping model. Each graph shows the best fit for selected inelastic collision energy barriers E_b . In the top curve, inelastic collisions are restricted to neighboring Zeeman states ($\Delta m_J = \pm 1$); in the bottom graph, all energetically accessible Zeeman states are included. The experimentally obtained data are shown in both graphs as solid squares.

be shorter than the time that a high-field seeking molecule needs to escape the trapping volume, a significant number of molecules can be repeatedly “switched” between *nontrappable* and *trappable* states. If this happens for many molecules of the ensemble, the observable lifetime is enhanced. This effect is more pronounced in the neighboring state model due to the fact that, if the collision energy is sufficient to reach the higher Zeeman level, there is always a 50% chance for a $\Delta m_J = +1$ transition. This is in contrast to the “all-inclusive” model where typically more transitions to lower states are possible, since these are energetically always allowed.

For CrH it can be seen in Fig. 5 that using *either* model, a satisfying match between simulated and experimental data can be obtained. One should note, however, that the energy barrier of 1 cm^{-1} for which the best agreement is obtained in the all-inclusive model rules out $\sim 70\%$ of the collisions at 650 mK.

For MnH, the all-inclusive model is not able to reproduce the observed buffer-gas density dependence of the trapping time, even at a relatively high energy barrier of 1.75 cm^{-1} . The neighboring states model, on the other hand, does give a good agreement with the observed data, including the rise in the trapping time for higher buffer-gas densities discussed above.

Based on these observations, we conclude that a model where only neighboring states are accessible in inelastic col-

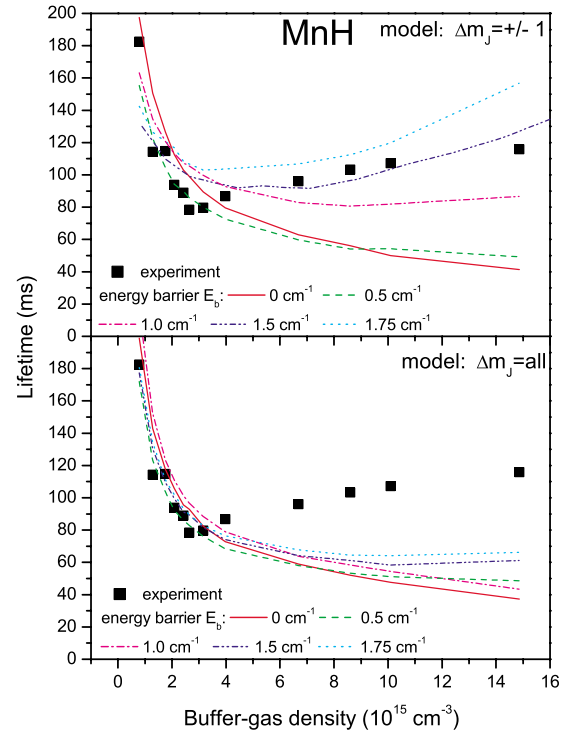


FIG. 6. (Color online) Simulated lifetime dependencies on the buffer-gas density of MnH, for two variants of the spin-flipping model. Each graph shows the best fit for selected inelastic collision energy barriers E_b . In the top curve, inelastic collisions are restricted to neighboring Zeeman states ($\Delta m_J = \pm 1$); in the bottom graph, all energetically accessible Zeeman states are included. The experimentally obtained data are shown in both graphs as solid squares.

lisions is the most suitable to describe Zeeman relaxation. With this, we obtain for CrH an inelastic collision cross section of $1.6 \times 10^{-18} \text{ cm}^2$, with an inelastic collision energy barrier E_b of 0.5 cm^{-1} . For MnH, we obtain an inelastic-scattering cross section of $3.1 \times 10^{-17} \text{ cm}^2$ at an inelastic collision energy barrier of 1.5 cm^{-1} . These values correspond to a gas temperature of 650 mK. The cross section for MnH is an order of magnitude larger than in the case of CrH, and leads to a lifetime extension at high buffer-gas densities due to an increased (back)conversion of the molecules from high-field-seeking to low-field-seeking behavior on their way toward the trap edge. It is difficult to give reliable uncertainties for the inelastic collision cross-section values given the very simplified inelastic scattering model. For CrH, we estimate the relative error to be about 30%. For MnH, where the match between theoretical model and measured data is worse, it should then be about 50%.

Figure 7 shows more detailed plots of the simulated CrH and MnH trapping times versus the buffer-gas density for which the best fits to our experimental data have been found. Here, it can be seen that the trapping time rises very fast at low buffer-gas densities, until reaching a sharp maximum at $\sim 0.5 \times 10^{15} \text{ cm}^{-3}$. After this, the trapping time gradually decreases over the buffer-gas range studied in this work and, for MnH, exhibits an increase above $\sim 4 \times 10^{15} \text{ cm}^{-3}$.

The maximum predicted trapping time of 250 ms for CrH could experimentally not be observed due to low signal

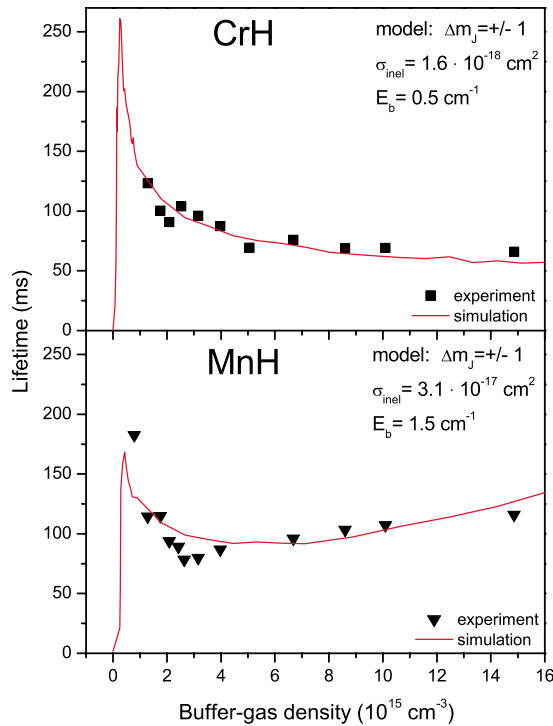


FIG. 7. (Color online) Calculated buffer-gas density dependence of the lifetimes of CrH and MnH molecules with inelastic-scattering cross sections of 1.6×10^{-18} and 3.1×10^{-17} cm^2 , respectively.

strength. As already mentioned, a certain buffer-gas density is needed for cooling a sufficient fraction of molecules before they are lost at the cell walls. From our simulations, we know that below a ^3He “threshold” buffer-gas density of $\sim 1.0 \times 10^{15}$ cm^{-3} hardly any molecules are translationally cooled. In addition to translational cooling, the molecules need to be cooled to the rotational ground state. Since we use this state for monitoring the relative number of molecules in the buffer-gas cell, this is a crucial process that presumably happens on a similar, but slightly longer, time scale than cooling of the translational motion. We therefore conclude that at buffer-gas densities of $\sim 0.5 \times 10^{15}$ cm^{-3} , for which these lifetimes are predicted, the number of collisions is insufficient to cool a sufficient fraction of molecules, both translationally and rotationally.

While the simulation for CrH shows an excellent agreement with the experimental data, the simulation for MnH exhibits shortcomings, especially seen in the pronounced dip in the observed trapping time around 3×10^{15} cm^{-3} . This is possibly caused by the oversimplified model of the Zeeman structure in the simulation, where the large density of Zeeman hyperfine states, induced by the nuclear spin ($I = \frac{5}{2}$) of the ^{55}Mn atom (abundance: 100%), is not implemented in the simulation. In addition to this, an inelastic collision energy barrier of 1.5 cm^{-1} is quite high, given the fact that all inelastic collisions induced by lower energies, and thus the majority of collisions, are simply not taken into account in our simple inelastic scattering model. Although the simulations give a good insight into the trapping dynamics of both molecules, it is clear that a theoretical study of the CrH-He and MnH-He collision processes, the inclusion of hyperfine

effects, rotational cooling, as well as the dependence of the cross sections on the magnetic field are required for a more quantitative model.

IV. CONCLUSION

We have buffer-gas cooled and magnetically trapped MnH and CrH molecules. In these experiments, maximum storage times of 120 ms (CrH) and 180 ms (MnH) at buffer-gas densities of $\sim 1 \times 10^{15}$ cm^{-3} were observed. At higher buffer-gas densities, Zeeman relaxation leads to lower trapping lifetimes which become comparable to the field-free diffusion times. To gain a better understanding of the trapping dynamics of MnH and CrH molecules, a numerical simulation was developed. Using a simplified phenomenological model where only energetically accessible spin-flipping transitions are allowed, inelastic and elastic collision cross sections are extracted. The model exhibits a good agreement with experimental data, and large inelastic-scattering cross sections have been found that seem to preclude the prolonged trapping and thermal isolation of samples in a buffer-gas cooling experiment.

The observed trapping dynamics are similar to those for NH in the buffer-gas cooling and trapping experiment by Doyle and co-workers [20]. For NH, a ratio of elastic-to-inelastic collisions of $\sim 7 \times 10^4$ was found. For CrH and MnH, we find significantly lower values of $\sim 9 \times 10^3$ (CrH) and $\sim 5 \times 10^2$ (MnH).

The storage times could be significantly enhanced when the helium gas is removed directly after the buffer-gas loading. Recently, it was shown that helium can be rapidly extracted from the trapping area [31]. As long as the removal time is shorter than the trapping time, this will considerably reduce trap loss due to inelastic helium-molecule collisions. In our magnetic trapping experiments on CrH and MnH, storage times exceeding 100 ms have been achieved. Since the buffer gas could be removed within a time of ~ 40 ms by means of a cryogenically driven active charcoal pump, this should be sufficient to achieve thermal disconnect between the molecular sample and the surrounding cell. Correspondingly, the implementation of this method seems crucial for the preparation of dense samples of trapped, isolated cold molecules using buffer-gas cooling. If the helium removal is successful, the trapping time also benefits from the fact that such a trapped sample is surrounded by a cryogenic environment at sub-Kelvin temperatures. This avoids trap loss via optical pumping induced by blackbody radiation, an effect that recently has been observed for molecules [32].

ACKNOWLEDGMENTS

We would like to thank John Doyle for his continuing support of this project, Wes Campbell and Nathan Brahm for fruitful discussions regarding inelastic collision properties of molecules, as well as Stephen Maxwell for providing us with parts of code that we used to build our own simulation. J.M.B. acknowledges funding through the European Network for Cold Molecules (RTN2-2001-00498).

- [1] J. J. Hudson, B. E. Sauer, M. R. Tarbutt, and E. A. Hinds, *Phys. Rev. Lett.* **89**, 023003 (2002).
- [2] D. Kwall, F. Bay, S. Bickman, Y. Jiang, and D. DeMille, *Phys. Rev. Lett.* **92**, 133007 (2004).
- [3] V. V. Flambaum and M. G. Kozlov, *Phys. Rev. Lett.* **98**, 240801 (2007).
- [4] E. R. Hudson, H. J. Lewandowski, B. C. Sawyer, and J. Ye, *Phys. Rev. Lett.* **96**, 143004 (2006).
- [5] J. J. Gilijamse, S. Hoekstra, S. Y. T. van de Meerakker, G. C. Groeneboom, and G. Meijer, *Science* **313**, 1617 (2006).
- [6] N. Balakrishnan and A. Dalgarno, *Chem. Phys. Lett.* **341**, 652 (2001).
- [7] R. V. Krems, *Int. Rev. Phys. Chem.* **24**, 99 (2005).
- [8] D. DeMille, *Phys. Rev. Lett.* **88**, 067901 (2002).
- [9] A. André, D. DeMille, J. M. Doyle, M. D. Lukin, S. E. Maxwell, P. Rabl, R. J. Schoelkopf, and P. Zoller, *Nat. Phys.* **2**, 636 (2006).
- [10] N. Vanhaecke, W. de Souza Melo, B. Laburthe Tolra, D. Comparat, and P. Pillet, *Phys. Rev. Lett.* **89**, 063001 (2002).
- [11] S. Jochim, M. Bartenstein, A. Altmeyer, G. Hendl, S. Riedl, C. Chin, J. Hecker Denschlag, and R. Grimm, *Science* **302**, 2101 (2003).
- [12] H. L. Bethlem, G. Berden, F. M. H. Crompvoets, R. T. Jongma, A. J. A. van Roij, and G. Meijer, *Nature* **406**, 491 (2000).
- [13] T. Junglen, T. Rieger, S. A. Rangwala, P. W. H. Pinkse, and G. Rempe, *Phys. Rev. Lett.* **92**, 223001 (2004).
- [14] M. S. Elioff, J. J. Valentini, and D. W. Chandler, *Science* **302**, 1940 (2003).
- [15] J. D. Weinstein, R. deCarvalho, T. Guillet, B. Friedrich, and J. M. Doyle, *Nature* **395**, 148 (1998).
- [16] J. D. Weinstein, R. deCarvalho, J. Kim, D. Patterson, B. Friedrich, and J. M. Doyle, *Phys. Rev. A* **57**, R3173 (1998).
- [17] J. Kim, B. Friedrich, D. P. Katz, D. Patterson, J. D. Weinstein, R. DeCarvalho, and J. M. Doyle, *Phys. Rev. Lett.* **78**, 3665 (1997).
- [18] C. I. Hancox, M. T. Hummon, S. V. Nguyen, and J. M. Doyle, *Phys. Rev. A* **71**, 031402(R) (2005).
- [19] C. I. Hancox, S. C. Doret, M. T. Hummon, L. J. Luo, and J. M. Doyle, *Nature* **431**, 281 (2004).
- [20] W. C. Campbell, E. Tsikata, Hsin-I Lu, L. D. van Buuren, and J. M. Doyle, *Phys. Rev. Lett.* **98**, 213001 (2007).
- [21] R. V. Krems, H. R. Sadeghpour, A. Dalgarno, D. Zgid, J. Klos, and G. Chalasinski, *Phys. Rev. A* **68**, 051401(R) (2003).
- [22] R. V. Krems, A. Dalgarno, N. Balakrishnan, and G. C. Groenenboom, *Phys. Rev. A* **67**, 060703(R) (2003).
- [23] H. Cybulski, R. V. Krems, H. R. Sadeghpour, A. Dalgarno, J. Klos, G. C. Groenenboom, A. van der Avoird, D. Zgid, and G. Chalasinski, *J. Chem. Phys.* **122**, 094307 (2005).
- [24] J. M. Bakker, M. Stoll, D. R. Weise, O. Vogelsang, G. Meijer, and A. Peters, *J. Phys. B* **39**, S1111 (2006).
- [25] *Gmelins Handbuch der Anorganischen Chemie—Cr-Teil B* (Verlag Chemie, Weinheim, 1966).
- [26] J. Chen, J. M. Bakker, A. Peters, M. Stoll, G. Meijer, and T. C. Steimle, *Phys. Chem. Chem. Phys.* **9**, 949 (2007).
- [27] T. C. Steimle, J. Gengler, M. Stoll, and G. Meijer, *J. Chem. Phys.* (to be published).
- [28] J. B. Hasted, *Physics of Atomic Collisions* (Elsevier, New York, 1972).
- [29] J. D. Weinstein, Ph.D. thesis, Harvard University, Cambridge, MA (2001).
- [30] J. D. Weinstein, R. deCarvalho, C. I. Hancox, and J. M. Doyle, *Phys. Rev. A* **65**, 021604(R) (2002).
- [31] J. G. E. Harris, R. A. Michniak, S. V. Nguyen, N. Brahm, W. Ketterle, and J. M. Doyle, *Europhys. Lett.* **67**, 198 (2004).
- [32] S. Hoekstra, J. J. Gilijamse, B. Sartakov, N. Vanhaecke, L. Scharfenberg, S. Y. T. van de Meerakker, and G. Meijer, *Phys. Rev. Lett.* **98**, 133001 (2007).